Using data assimilation to understand the effect of disturbance on a managed woodland DRAFT

Ewan Pinnington

October 31, 2016

Abstract

The response of forests and terrestrial ecosystems to disturbance is an important process in the global carbon cycle in the context of a changing climate. Disturbance can take many forms, for example; felling, fire and insect outbreak. In current estimates of the global carbon budget, disturbance is one of the least understood components. In this paper, we investigate the effect of the management practice f selective felling on the carbon dynamics of a mature temperate woodland. In order to better understand ecosystem response we use the mathematical technique of data assimilation to combine a diverse set of observations with a mathematical model of ecosystem carbon balance. Data assimilation combines the uncertainty from observations and prior model predictions to find the best possible estimate to the studied system. We develop new data assimilation techniques allowing for the assimilation of daytime and nighttime net ecosystem exchange observations with a daily time-step model. This allows for the assimilation of much otherwise neglected carbon flux information. The presented techniques allow us to estimate the effect of step-changes in ecosystem composition on the parameter and state variables in a modelled estimate of forest carbon balance. These techniques are applicable to other ecosystem models and data assimilation schemes. Previous statistical analyses of eddy covariance data at the study site had suggested that disturbance from selective felling (thinning) resulted in no change to the net carbon uptake of the ecosystem. We show that this is likely due to reduced ecosystem respiration post-disturbance compensating for a reduction in gross primary productivity. Our results support the theory of an upper limit of forest net carbon uptake due to the magnitude of ecosystem respiration scaling with gross primary productivity.

1 Introduction

1.1 Role of disturbance in the global C cycle

Disturbances to terrestrial ecosystems (e.g. felling, fire or insect outbreaks) can have significant effects on net land surface carbon uptake. The response of forests and terrestrial ecosystems to disturbance is one of the least understood components in the global carbon cycle [Ciais et al., 2014]. Land surface models fail to represent the effect of disturbances on long-term carbon dynamics [Running, 2008]. The disturbance of forests can have varying degrees of severity; ranging from stand replacing disturbance, where tree mortality is close to 100%, to non-stand replacing disturbance, where a proportion of total trees are lost.

1.2   Current theories on terrestrial ecosystem response to disturbance

In this paper we investigate the effect of selective felling (thinning) on the carbon dynamics of a mature deciduous forest stand. Thinning is a globally widespread silvicultural practice used to improve ecosystem services or the quality of a final tree crop. The effect of thinning on carbon budgets has largely been ignored [Liu et al., 2011]. It would be logical to assume that after thinning we would see a reduction in the net carbon uptake of an ecosystem. Presumably due to reduced Gross Primary Productivity (GPP) following a reduction in total leaf area and unchanged or heightened ecosystem respiration due to an input of brash and woody debris to the forest floor. However, previous studies, analysing flux-tower eddy covariance records, find no significant change in the observed net ecosystem exchange (NEE) of CO_2 after thinning [Dore et al., 2012, Moreaux et al., 2011, Vesala et al., 2005, Wilkinson et al., 2015]. These studies suggest this is due to increased light availability and reduced competition allowing ground vegetation to display increased GPP and compensate for an increase in heterotrophic respiration post-disturbance.

Other studies have shown a significant reduction in the carbon content of rhizosphere soils following tree felling [Hernesmaa et al., 2005]. It has been shown that tree roots provide a rhizosphere priming effect, greatly increasing the rate of soil organic carbon decomposition [Dijkstra and Cheng, 2007], suggesting a decrease in respirations following thinning. This is consistent with work carried out at the study site of focus in this paper, where it has been shown that the magnitude of ecosystem respiration is strongly coupled to the magnitude of GPP [Heinemeyer et al., 2012]. Predictions made by Kurz et al. [2008] about the impacts of mountain pine beetle outbreaks in Northern America estimated the migration of forests from sinks to sources of carbon following this insect disturbance. However, the analysis of a diverse set of observations for an area with approximately 70% infested trees by Moore et al. [2013] revealed little change in net CO_2 flux, due to concurrent reductions in gross primary productivity and ecosystem respiration. Similar results are also found from large scale tree girdling experiments [Högberg et al., 2001], where 1-2 months after girdling a 54% decrease in soil respiration is observed.

1.3   The role of data assimilation for improving estimates to a system

Data assimilation is a mathematical technique for combing observations with prior model predictions in order to find the best estimate to a studied system. Functional ecology models have been combined with many different observations relevant to the carbon balance of forests [Fox et al., 2009, Niu et al., 2014, Quaife et al., 2008, Richardson et al., 2010, Zobitz et al., 2011, 2014]. Leading to improved estimates of model parameter and state variables and reduced uncertainty in model predictions. Although there has been many efforts to model the effect of disturbance on forest ecosystems [Seidl et al., 2011, Thornton et al., 2002], the use of data assimilation has been limited, with only a few examples using satellite data [Hilker et al., 2009, Kantzas et al., 2015]. The authors are not aware of any studies assimilating site level data to quantify disturbance effects. By assimilating observations relevant to post-disturbance ecosystem carbon dynamics with prior model predictions of ecosystem behaviour, we can analyses the retrieved parameters after data assimilation to find the model predicted effects of disturbance.

1.4   What does this paper do?

In this paper we investigate the effect of thinning on the carbon dynamics of the Alice Holt flux site [Wilkinson et al., 2012], a deciduous managed woodland. We investigate an event that occurred in 2014, when one side of the site was thinned and the other side left unmanaged. During this thinning approximately 46% of trees were removed from the studied area. In order to better understand the

effect this thinning had on stand structure an intensive field campaign was undertaken in 2015 to measure leaf area index and also estimate woody biomass for both sides of the study site. The site has a flux tower positioned on the boundary between the thinned and unthinned forest. The eddy covariance record of NEE was split between the two sides using a flux footprint model. Previous statistical analysis of a thinning event in 2007 had suggested that there was no change in NEE between the thinned and unthinned sides of the forest post-disturbance [Wilkinson et al., 2015].

We present new methods for the assimilation of daytime and nighttime NEE observations with a daily time-step model, in this case the Data Assimilation Linked Ecosystem Carbon (DALEC2) model [Bloom and Williams, 2015]. These methods require no model modification. We combine all available observations for 2015 with prior model predictions to find two sets of optimised model parameter and initial state values, corresponding to thinned and unthinned sides of the forest. We then use these two versions of the model to seek an explanation for why the net uptake of carbon remains unchanged even after removing a large proportion of the trees from one side. The data assimilation techniques presented in this paper could be applied for similar analyses at other sites and provide a novel method to help elucidate the reasons behind ecosystem responses.

2 Observation and data assimilation methods

2.1 Alice Holt research forest

Alice Holt Forest is a research forest area managed by the UK Forestry Commission located in Hampshire, SE England. Forest Research has been operating a CO_2 flux measurement tower in a portion of the forest, the Straits Inclosure, since 1998. It is one of the longer forest site CO_2 flux records, globally. The Straits Inclosure is a 90 ha area of deciduous broadleaved plantation woodland on a surface water gley soil, which has been managed for the past 80 years. The majority of the canopy trees are oak (*Quercus robur* L.), with an understory of hazel (*Corylus avellana* L.) and hawthorn (*Crataegus monogyna* Jacq.); but there is a small area of conifers (*Pinus nigra* J. F. Arnold) within the tower measurement footprint area in some weather conditions. Further details of the Straits Inclosure site and the measurement procedures are given in Wilkinson et al. [2012], together with analysis of stand-scale 30 minute average net CO_2 fluxes (NEE) measured by standard eddy covariance methods from 1998-2011.

As part of the management regime, the Straits Inclosure is subject to thinning; whereby a proportion of trees are removed from the canopy in order to reduce competition and improve the quality of the final tree crop. At the Straits an intermediate thinning method is used with a portion of both subdominant and dominant trees being removed from the stand [Kerr and Haufe, 2011]. The whole of the stand was thinned in 1995. Subsequently the Eastern side of the Straits was thinned in 2007 and then the Western side in 2014. The flux tower at the site is situated on the boundary between these two sides, allowing for the use of a footprint model to split the flux record and analyse the effect of this disturbance on carbon fluxes at the site. In Wilkinson et al. [2015] a statistical analysis of the eddy covariance flux record found that there was no significant effect on the net carbon uptake of the Eastern side after thinning in 2007. In this paper we focus on the effect of disturbance on the Western side after thinning in 2014. We therefore refer to the Western side as thinned and the Eastern side as unthinned.

2.2 Observations

In order to assess the effect the 2014 thinning had on the Straits Inclosure an intensive field campaign was undertaken in 2015 to measure leaf area index and also estimate woody biomass. From the

site we also have a long record of flux data as discussed in section 2.1. These observations span both the thinned and unthinned sides of the forest and give us two distinct sets of observations describing both sides of the site.

2.2.1 Flux tower eddy covariance

The Straits Inclosure flux tower provides us with half-hourly observations from January 1999 to December 2015, these consist of the NEE fluxes and meteorological driving data of temperature, irradiance and atmospheric CO_2 concentration for use in the DALEC2 model. The NEE data is subject to u^* filtering and quality control procedures as described by Papale et al. [2006], but is not gap-filled. The resultant half-hourly NEE dataset is then split between observations corresponding to the Western thinned and Eastern unthinned sides of the site using a flux-footprint model, see Wilkinson et al. [2015] for more details.

In data assimilation NEE observations are usually averaged daily for use with daily time-step functional ecology models. To compute daily NEE observations we take the mean over the 48 measurements made each day, selecting only days where there is no missing data. As we have been strict on the quality control of the flux record and not allowed any gap filling this presents a problem in the number of NEE observations available to us. By splitting the flux record between two sides we retrieve very few total daily observations of NEE. In order to address this we instead compute day and nighttime NEE fluxes (NEE_{day} and NEE_{night} respectively) for use in data assimilation. To compute daytime or nighttime NEE observations, we take the mean over the half-hourly day or nighttime (calculated using a solar model) measurements, again only taking periods where there are no gaps in the data so that we are only considering true observations. This provides us with many more observations for assimilation after data processing, as seen in table 1. Because we are averaging over shorter time periods we have a smaller probability of gaps and erroneous data. We see that we have many more daytime NEE observations than nighttime, as we tend to have much more turbulent air mixing in daylight hours. In section 2.3.2 we give details of how we relate these twice daily observations of NEE to a daily time-step model.

Sector	NEE	NEE_{day}	NEE_{night}
Unthinned (E)	8	43	10
Thinned (W)	8	49	24

Table 1: Number of observations of NEE, NEE_{day} and NEE_{night} for East and West sides of the Straits Inclosure for the year 2015.

In Richardson et al. [2008] the error in observations of daily NEE is found to be between 0.2 to 0.8 g C m^{-2}day^{-1}. Richardson et al. [2008] also show that flux errors are heteroscedastic. In Williams et al. [2005] errors in NEE are assumed to be constant and set at 0.5 g C m^{-2}day^{-1}. To account for the heteroscedastic nature of NEE errors we define an error function that scales between 0.5 to 0.8 g C m^{-2}day^{-1} based on the magnitude of the observation. This function is defined as $0.5 + 0.03|NEE_{day}^i|$ g C m^{-2}day^{-1}, where $|NEE_{day}^i|$ is the magnitude of the daytime NEE observation. Raupach et al. [2005] comment that nighttime measurements of NEE are much more uncertain than daytime measurements. This is difficult to quantify, but here we assume that nighttime flux errors are 3 times the magnitude of daytime errors. We therefore have the error function of $1.5 + 0.09|NEE_{night}^i|$ g C m^{-2}day^{-1}, where $|NEE_{night}^i|$ is the magnitude of the nighttime NEE observation. We also include correlations in time between the errors in our observations of NEE, as discussed in Pinnington et al. [2016].

2.2.2   Leaf area index

As part of the work undertaken for this paper; to assess the impact of the 2014 thinning, three transects were established in the Straits Inclosure for intensive sampling during 2015. A total of 435 sampling points were marked at 10 m apart, using a GPS unit and fluorescent tree spray paint. Measurements of peak LAI (July 2015 - September 2015) were made using both a ceptometer and hemispherical photography. The transects were walked twice with the ceptometer, sampling every 10 m, giving 870 readings in total. Hemispherical photographs were taken every 50 m as shown in Figure 1, giving 89 photographs in total.

The ceptometer is used with an additional Photosynthetically Active Radiation (PAR) sensor. We measure below canopy PAR using the ceptometer while logging above canopy PAR using a data logger and PAR sensor positioned outside the canopy. We can then estimate LAI using the above and below canopy readings and a set of equations relying on some assumptions [Fassnacht et al., 1994]. For the hemispherical photographs, we use the HemiView software [Rich et al., 1999] which can calculate the proportion of visible sky as a function of sky direction (gap fraction) this can then be used to calculate LAI [Jonckheere et al., 2004].

Six litter traps were also established at points along the transects allowing for comparison with the other methods. These were sampled throughout the season in 2015. We found the litter trap derived LAI was always greater than LAI estimates derived from optical methods, as expected [Bréda, 2003]. From the sampling of the litter traps we also have estimates to leaf mass per area for use in data assimilation. As the 6 litter traps are not enough to describe the LAI for the research site [Kimmins, 1973], we used estimates from the ceptometer and hemispherical photographs for data assimilation. We take the weighted average of the hemispherical photograph and ceptometer estimated LAI to find an LAI of 4.42 with a standard error of 0.07 for the Eastern unthinned section of forest, and an LAI of 3.06 with a standard error of 0.07 for the Western thinned section of forest. We are assimilating the mean of 299 LAI observations in the unthinned and 225 in the thinned section of forest. Consequently the appropriate representation of error for data assimilation is the standard error of the mean. From our litter trap observations we find a leaf mass per area of 29 g C m^{-2} for both sides of the forest.

2.2.3   Woody biomass

The method of Point-Centred Quarters (PCQ) was used to conduct a biomass survey as specified in Dahdouh-Guebas and Koedam [2006]. 114 points were sampled along the three transects measuring the Diameter at Breast Height (DBH) and the density of trees. We then used allometric relationships between DBH and total above ground biomass and coarse root biomass, found in work carried out by Forest Research and in McKay et al. [2003], to find an estimate to total woody and coarse root carbon. We can see these observations in table 2, we have made the assumption that 50% of dry plant mass is carbon.

Forest Research also carry out their own mensuration studies at the site. One such study was carried out of the Western side after the thinning at a similar time to our own PCQ measurements and found a tree density of 225 ha^{-1} and an average DBH of 32 cm, which are in close agreement to our own estimates in table 2. This gives us confidence that past measurements before the thinning will also be representative of the methods we have used. From 2009, measurements from Forest Research found the Western side to have a tree density of 418 ha^{-1} and an average DBH of 27.73 cm. This suggests that approximately 46% of trees have been removed during thinning. From these estimates we can also see the effect thinning has on the type of trees found at the site. The amount of trees per hectare has dropped dramatically after thinning but the mean DBH has increased,
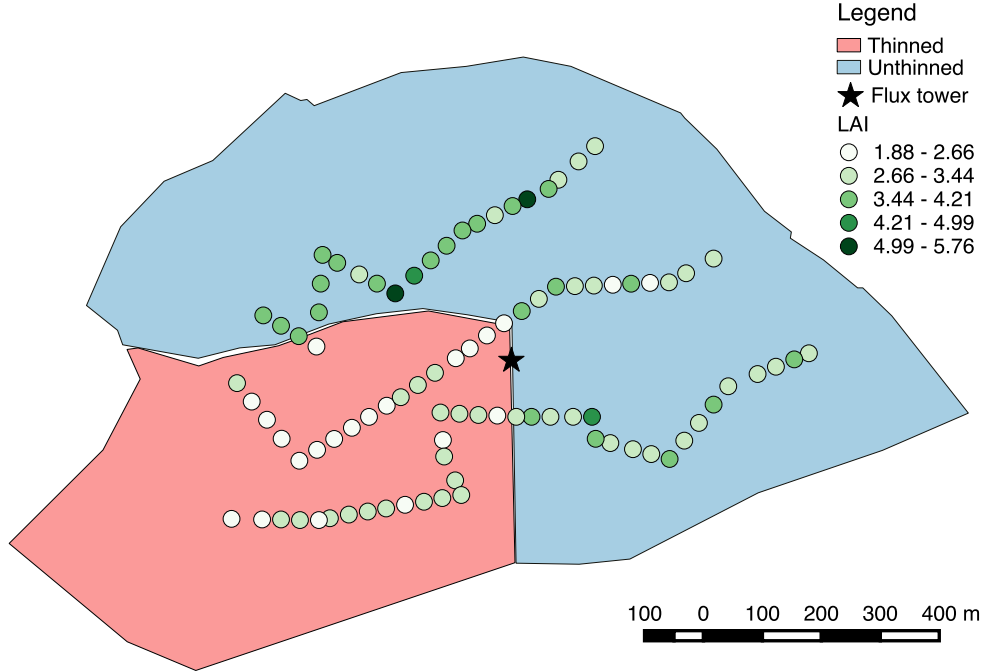
Figure 1: Hemispherical photograph derived LAI for the Straits Inclosure at 50m intervals along three transects.

indicating that smaller subdominant trees have been removed. The mean DBH on the Eastern side is greater still, indicating that the thinning that took place in 2007 of the Eastern side has allowed the dominant trees to grow as a result of reduced competition.

Sector	Tree density (ha^{-1})	mean DBH (cm)	Estimated Woody biomass and coarse root carbon (g C m^{-2})
Unthinned (E)	272	34.12	13130
Thinned (W)	225	32.85	9908

Table 2: Point-centred quarter method observations for 2015.

2.3 Model and data assimilation

2.3.1 DALEC2 ecosystem carbon model

The DALEC2 model is a simple process-based model describing the carbon dynamics of a forest ecosystem [Bloom and Williams, 2015]. The model is constructed of six carbon pools (labile (C_{lab}), foliage (C_f), fine roots (C_r), woody stems and coarse roots (C_w), fresh leaf and fine root litter (C_l) and soil organic matter and coarse woody debris (C_s)) linked via fluxes. The aggregated canopy model (ACM) [Williams et al., 1997] is used to calculate daily gross primary production (GPP) of the forest, taking meteorological driving data and the modelled leaf area index (a function of C_f) as arguments. Figure 2 shows a schematic of how the carbon pools are linked in DALEC2, full model equations can be found in the appendix, section 6.
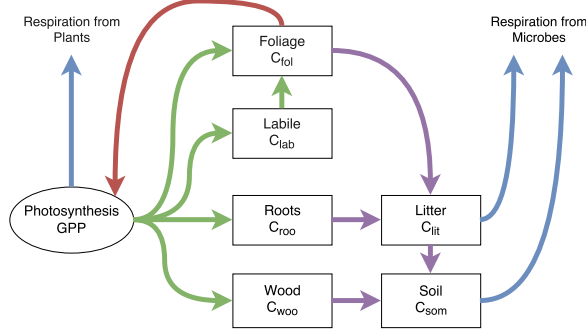
Figure 2: Representation of the fluxes in the DALEC2 carbon balance model. Green arrows represent C allocation, purple arrows represent litter fall and decomposition fluxes, blue arrows represent respiration fluxes and the red arrow represents the influence of leaf area index in the GPP function.

2.3.2 Data assimilation

We implement Four-Dimensional Variation data assimilation (4D-Var) with the DALEC2 model for joint parameter and state estimation. In 4D-Var we aim to find the parameter and initial state values such that the model trajectory best fits the data over some time window, given some prior information about the system. This prior information takes the form of an initial estimate to the parameter and state variables of the model, $\mathbf{x}^b$, valid at the initial time. This prior is assumed to have unbiased, Gaussian errors with known covariance matrix $\mathbf{B}$. Adding the prior term ensures that our problem is well posed and that we can find a locally unique solution [Tremolet, 2006]. The prior used in this paper is derived from the assimilation of eddy covariance data from previous years and can be found in table 3. In 4D-Var we aim to find the parameter and initial state values that minimises the weighted least squares distance to the prior, while minimising the weighted least squares distance of the model trajectory to the observations over the time window $t_0, \ldots, t_N$ [Lawless, 2013]. We do this by finding the state $\mathbf{x}^a$ at time t_0 that minimises the cost function

$$J(\mathbf{x}_0) = \frac{1}{2}(\mathbf{x}_0 - \mathbf{x}^b)^T \mathbf{B}^{-1}(\mathbf{x}_0 - \mathbf{x}^b) + \frac{1}{2}\sum_{i=0}^{N}(\mathbf{y}_i - \mathbf{h}_i(\mathbf{x}_i))^T \mathbf{R}_i^{-1}(\mathbf{y}_i - \mathbf{h}_i(\mathbf{x}_i)), \tag{1}$$

where $\mathbf{x}_0$ is the vector of parameter and initial state values to be optimised, $\mathbf{h}_i$ is the observation operator mapping the parameters and state to the observations $\mathbf{y}_i$ and $\mathbf{R}_i$ is the observation error covariance matrix. Further details of the implemented data assimilation scheme and specification of prior and observational errors can be found in Pinnington et al. [2016].

In this paper we assimilate day and nighttime NEE in order to increase the number of observations available to us and also better partition our modelled estimate of GPP and total ecosystem respiration, as discussed in section 2.2.1. As the DALEC2 model runs at a daily time step, this requires us to relate the daily parameter and state values from the model to the twice-daily observations of NEE. We do this by writing two new observation operators, one relating the model state and parameters to daytime NEE, and the other to nighttime NEE. The NEE of CO_2 at any given time is the difference between GPP and ecosystem respiration. For an observation of total daily NEE on day i we have,

$$NEE^i = -GPP^i(C_{fol}^i, \Psi) + f_{auto}GPP^i(C_{fol}^i, \Psi) + \theta_{lit}C_{lit}^i e^{\Theta T^i} + \theta_{som}C_{som}^i e^{\Theta T^i}, \tag{2}$$

7

where all terms have the same meaning as described in section 6, with term one being gross primary productivity, term two corresponding to autotrophic respiration and term three and four corresponding to heterotrophic respiration. For total daytime NEE we have,

$$NEE_{day}^i = -GPP^i(C_{fol}^i, \Psi) + \delta_{day} f_{auto} GPP^i(C_{fol}^i, \Psi) + \delta_{day}\theta_{lit}C_{lit}^i e^{\Theta T_{day}^i} + \delta_{day}\theta_{som}C_{som}^i e^{\Theta T_{day}^i}$$
(3)

where δ_{day} is the day length, expressed as $\frac{\text{number of daylight hours}}{24}$, and T_{day}^i is the mean daytime temperature. Here we still have the same term for GPP as in equation (2) as all photosynthesis occurs during daylight hours, the respirations are then scaled by the length of daylight hours. For nighttime NEE we have,

$$NEE_{night}^i = \delta_{night} f_{auto} GPP^i(C_{fol}^i, \Psi) + \delta_{night}\theta_{lit}C_{lit}^i e^{\Theta T_{night}^i} + \delta_{night}\theta_{som}C_{som}^i e^{\Theta T_{night}^i}$$
(4)

where δ_{night} is the night length, expressed as $\frac{\text{number of night hours}}{24}$, and T_{night}^i is the mean nighttime temperature. Here we no long have a term for GPP as no GPP will occur during the night. The respirations are again scaled by night length as in equation (3). Day length and night length are calculated using a solar model here, but could also be estimated using the record of incident solar radiation from the flux tower. These new observation operators allow for assimilation of day/nighttime NEE without the need for model development and can be applied to other ecosystem models to allow for the assimilation of finer temporal resolution eddy covariance data and possible improvements to the partitioning of photosynthesis and ecosystem respiration. From section 3 we can see that these modified observation operators allow our model to predict both daytime and nighttime NEE accurately.

2.4 Experimental setup

Using the prior model estimate specified in table 3, we run two data assimilation experiments for the years window of 2015. In the first experiment we assimilated all data available (as specified in section 2.2) for the unthinned Eastern section of forest. In the second experiment we assimilate all data available for the thinned Western section of forest. Combining these two distinct sets of observations with our prior model using 4D-Var data assimilation allows us to retrieve two unique sets of parameter and initial state values, corresponding to the thinned and unthinned sections of the site. This allows us to judge the effect the thinning in 2014 had on the carbon dynamics of the forest in 2015. We do this by analysing the optimised parameter and initial state values for the thinned and unthinned sections of the forest and also considering the model predictions of different variables for each side post-disturbance.

3 Results

In Figure 3 we show the observations and model trajectories after assimilation for both thinned and unthinned sections of the forest site. We can see that we fit all the observations well after assimilation. We have confidence in our results as we know that even assimilating a single year of data we can accurately describe the carbon uptake of the site for a long time period (15 years) into the future [Pinnington et al., 2016]. From Figure 3a and 3b the modified observation operators presented in section 2.3.2 have allowed our model to represent both daytime and nighttime NEE well.

From Figure 3c and 3d the distinct difference in stand structure is clear with reduced LAI and woody carbon for the thinned area. The model predicted time of green-up and senescence

in LAI is consistent with phenocam observations made by Forest Research at the site (maybe include phenocam plot for 2015 in sup. material?). In Figure 3a we see that both model predicted and observed net carbon uptake of both the thinned and unthinned is very similar. The model predictions of NEE_{day} are overlapping for most of the 2015 window. However, in Figure 3b we see that our model predicts reduced reduced NEE_{night} for the thinned compared to unthinned, here NEE_{night} correspond to ecosystem respiration as no GPP occurs during the night.

(a) NEE_{day}

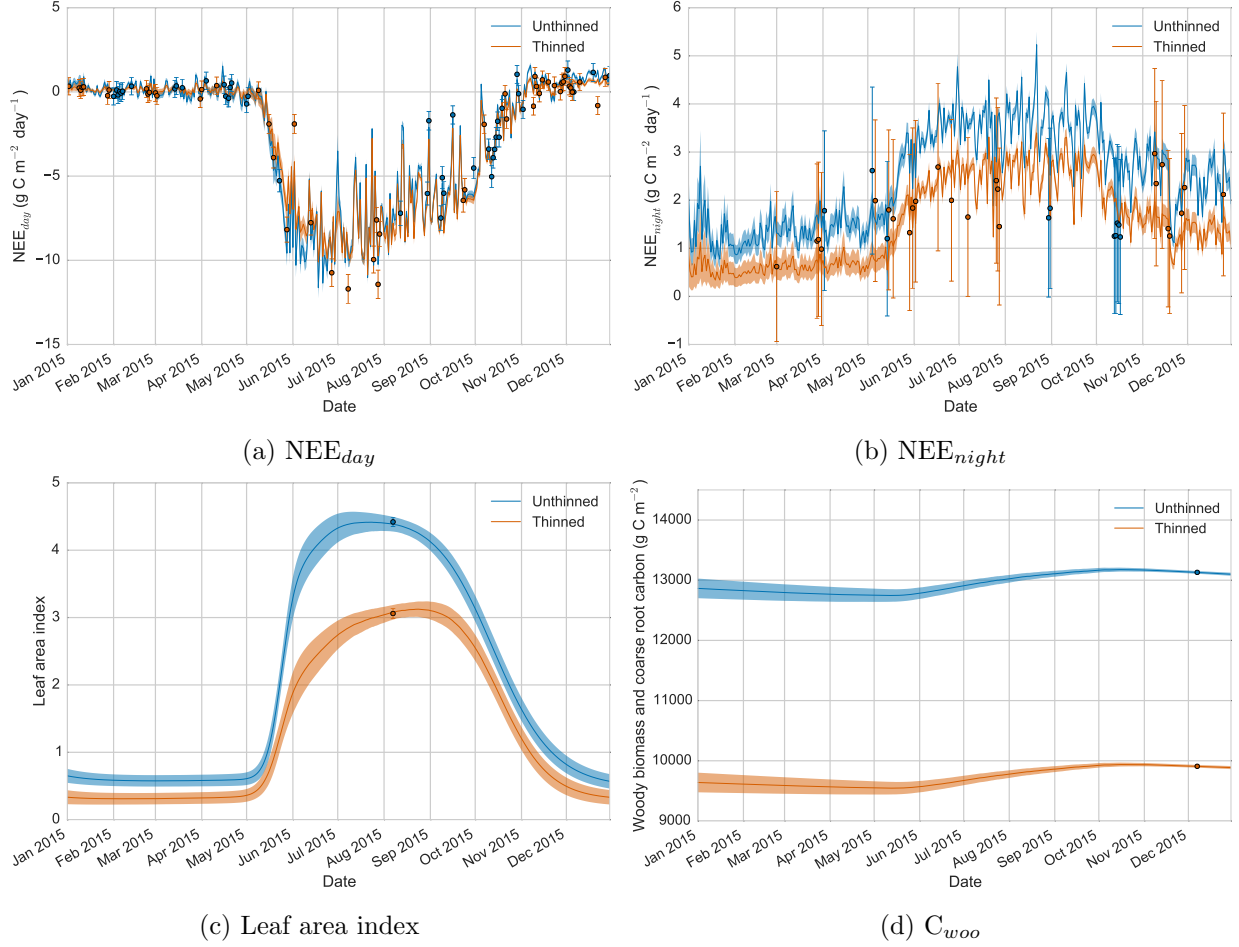(b) NEE_{night}

(c) Leaf area index

(d) C_{woo}

Figure 3: 2015 unthinned and thinned observations and model trajectories after assimilation. Blue line: model trajectory after assimilation of unthinned data, blue shading: uncertainty in model trajectory after assimilation ($\pm$ 1 standard deviation), blue dots: unthinned observations with error bars, orange line: model trajectory after assimilation of thinned data, orange shading: uncertainty in model trajectory after assimilation ($\pm$ 1 standard deviation), orange dots: thinned observations with error bars.

In Figure 6 we show the model predicted GPP and ecosystem respiration (including its partitioning between autotrophic and heterotrophic) for both thinned and unthinned after data assimilation. Figure 6a shows the model predicting a reduction in GPP following a reduction in leaf area for the thinned. In order to compensate for this reduced GPP, in Figure 6b we see the thinned is demonstrating reduced total ecosystem respiration, this allows the thinned to still do the same net carbon uptake as the unthinned (seen in Figure 3a), as net ecosystem carbon uptake = - GPP + ecosystem respiration. From Figure 4c and 4d we see that heterotrophic respiration sees the

greatest reduction compared to the unthinned, however autotrophic respiration is also reduced.

(a) GPP

(b) Total ecosystem respiration

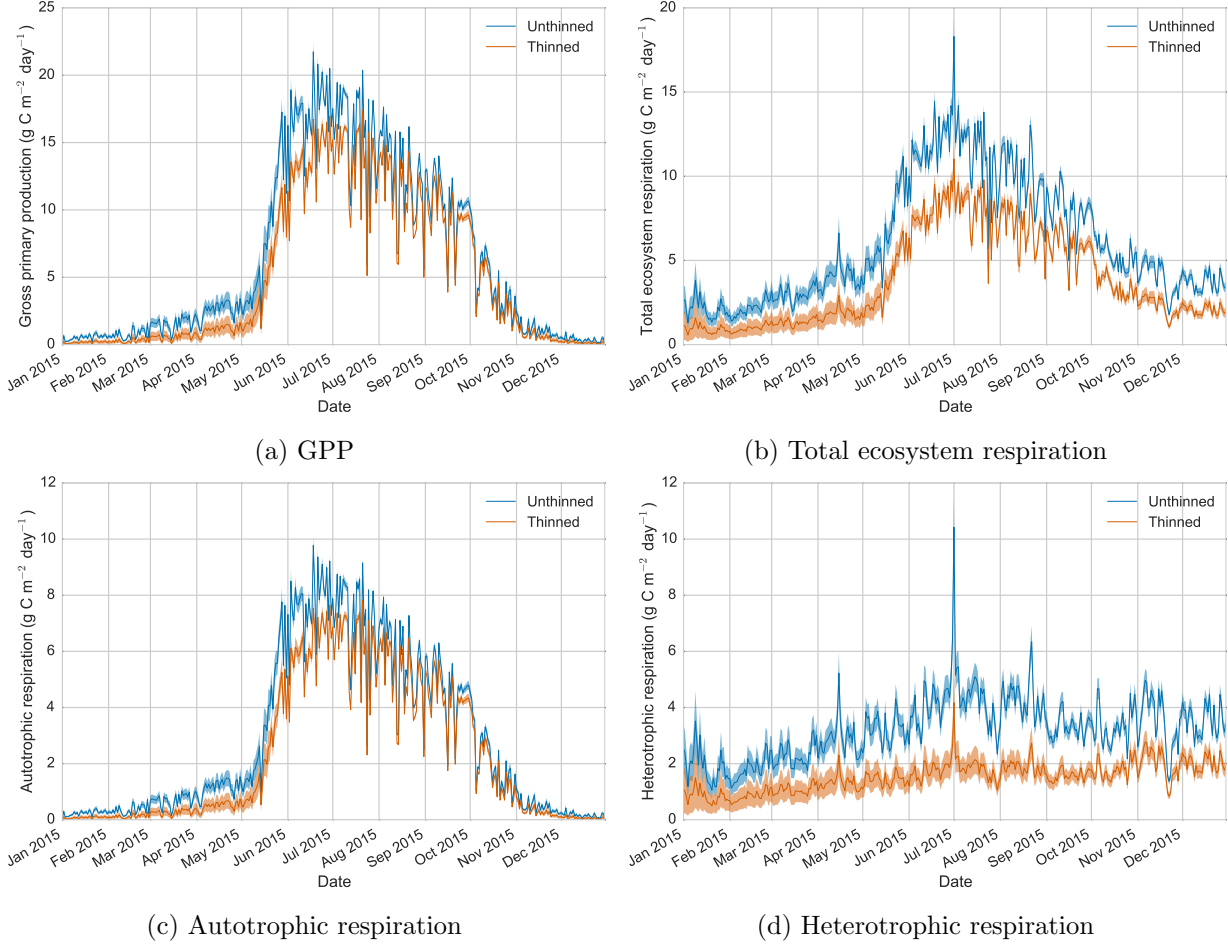(c) Autotrophic respiration

(d) Heterotrophic respiration

Figure 4: 2015 unthinned and thinned model trajectories after assimilation. Blue line: model trajectory after assimilation of unthinned data, blue shading: uncertainty in model trajectory after assimilation ($\pm$ 1 standard deviation), orange line: model trajectory after assimilation of thinned data, orange shading: uncertainty in model trajectory after assimilation ($\pm$ 1 standard deviation).

Figure 5 shows the change in parameter and initial state values for thinned and unthinned after assimilating the 2015 data. It is important to note this is the difference when compared to our prior model estimate, which was found by assimilating only eddy covariance data from previous years, and a single observation of leaf mass per area estimated from Forest Research litter traps. We therefore expect changes in parameter and state values for both thinned and unthinned, as we are assimilating new data streams. This is particularly noticeable in the carbon pool state members in Figure 5. Constraints on the carbon pool state members are provided by the assimilated observations of woody biomass and coarse roots (C_{woo}), LAI and leaf mass per area (c_{lma}). LAI and c_{lma} give us a constraint on foliar carbon (C_{fol}) as LAI $= \frac{C_{fol}}{c_{lma}}$. We can see the values for the model predicted carbon pools are as we might expect with the thinned having less carbon in all pools compared to the unthinned. For litter carbon (C_{lit}) it is possible that the input of brash and woody debris may compensate for the reduction in input of leaf litter on the thinned side. However, this woody debris is much less readily decomposed and so possibly has little impact in the year after thinning. We also see a large difference in the predicted soil carbon content (C_{som})

10

between the two model predictions. This is consistent with studies analysing soil carbon contents after felling [Hernesmaa et al., 2005].

For the parameters the biggest changes appear to be in the litter mineralisation parameter (θ_{min}) and the fraction of GPP allocated to foliage (f_{fol}). θ_{min} is a parameter that our results are relatively insensitive to, as it is a very slow process which we do not have much information about after assimilating only a single years data. Our model predicted LAI seems unaffected by f_{fol}, as we are modelling a deciduous forest it relies more on the flow of labile carbon to the leaves at green-up than the input of GPP, this can be seen in equations (6) and (7) in the appendix. We also see a distinct difference in the parameter controlling the rate of soil carbon turnover (θ_{som}), with this parameter being smaller for the thinned side of the forest. This could occur due to a reduction in the priming of rhizosphere soils [Dijkstra and Cheng, 2007], since almost half of the trees have been lost in the thinned section.
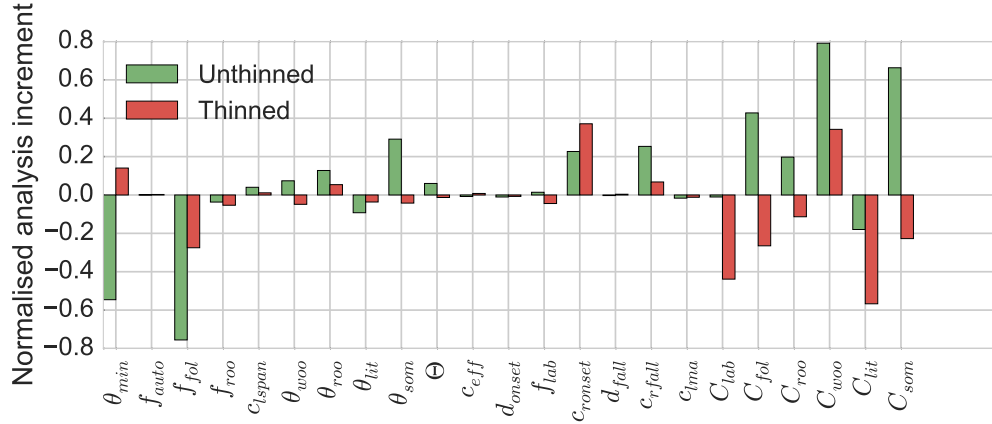

Figure 5: Normalised analysis (posterior model) increment $\left(\frac{(\mathbf{x}^a - \mathbf{x}^b)}{\mathbf{x}^b}\right)$ for the East and West experiments. Explanation of parameter and state variable symbols in table 3.

4   Discussion

In this paper we have used data assimilation to combine observations and prior model predictions of ecosystem carbon balance in order to understand how the state of an ecosystem might be altered after a disturbance event. We find no significant change in net carbon uptake for the studied ecosystem following stand thinning, where approximately 46% of trees were removed. This is consistent with other studies of ecosystem carbon dynamics following thinning. We find evidence that reductions in GPP following a decrease in total leaf area post-thinning are being offset by simultaneous reductions in ecosystem respiration. This is in contrast to current suggestions that reduced canopy photosynthesis is compensated for by increased GPP by ground vegetation post-thinning [Dore et al., 2012, Moreaux et al., 2011, Vesala et al., 2005, Wilkinson et al., 2015]. However does support work investigating the effect of insect disturbance [Moore et al., 2013].

Our results show a decrease in both autotrophic and heterotrophic respirations following thinning. Autotrophic respiration has both above and below ground components, whereas heterotrophic respiration is mainly from soils and litter. There is no set definition for below ground autotrophic respiration but it is often characterised as respiration from roots, mycorrhizal fungi and other micro-organisms dependent on the priming of soils with labile carbon compounds from roots. It has been shown recently that deep root systems and their influences may be more widespread than

previously thought [Pierret et al., 2016]. Heterotrophic respiration is respiration by microbes not directly dependent on autotrophic substrate, however the largest fraction of heterotrophic respiration is based on the decomposition of young organic matter (e.g. leaves and fine roots) whose availability also depends on the GPP of an ecosystem [Janssens et al., 2001]. We find the largest decreases in heterotrophic respiration compared to autotrophic respiration. While it has been shown that heterotrophic respiration can decrease after disturbance events [Bhupinderpal et al., 2003], it is possible we overestimate the reduction in heterotrophic respiration and underestimate the reduction in autotrophic respiration. This is understandable as we have assimilated no data on this partitioning. Also our model description of autotrophic respiration is simple (described as a constant fraction of GPP) and therefore the models heterotrophic component might compensate and in this instance describe the behaviour of mycorrhizal fungi and other microbes commonly categorised in the autotrophic component of respiration.

In a study measuring soil CO_2 fluxes over 4 years at the Straits Inclosure (the study site in this paper) Heinemeyer et al. [2012] showed a large 56% contribution of autotrophic respiration (characterised as root and mycorrhizal respiration) to total measured soil respiration. Heinemeyer et al. [2012] also suggested that mycorrhizal fungi play a role in priming the turnover of soil organic carbon by other microbes, with evidence from other studies [Talbot et al., 2008]. Högberg and Read [2006] find similar figures for the autotrophic contribution to total soil respiration, with around half or more of all soil respiration being driven by recent photosynthesis. Heinemeyer et al. [2012] discuss the possibility of this tight coupling between GPP and ecosystem respiration leading to an upper limit for forest CO_2 uptake due to increased GPP leading to increased respiration, this is also discussed by Heath et al. [2005]. Our results support this theory, as we see ecosystem respiration scaling with GPP after approximately 46% of trees are removed from the study site, meaning that we find no significant change in net ecosystem carbon uptake after thinning.

Studies analysing eddy covariance flux records also find no change in the net ecosystem exchange of CO_2 after thinning [Dore et al., 2012, Moreaux et al., 2011, Vesala et al., 2005, Wilkinson et al., 2015]. These studies suggest that this is due to increased GPP by ground vegetation (following increased light availability and reduced competition) compensating for increases in heterotrophic respiration and reduced canopy photosynthesis post-thinning. We do not find evidence to support this and instead suggest that reduced ecosystem respiration is the most important component for the unchanged NEE of the forest following thinning. However, it is important to note that our observations of LAI are made at approximately 1 m above the forest floor. This means that our observations of LAI do not account for ground vegetation and therefore any effect of this ground vegetation is not simulated by our model. Despite this, observations made during multiple walks of the three established transects find no evidence of increased ground vegetation in the year after thinning. In fact much of the ground vegetation and subcanopy was removed during thinning and does not appear to have recovered in the following year. At longer time-scales we believe re-growth of the subcanopy and ground vegetation will play an important role in increased productivity. Our results suggest that this increased productivity would also be met with subsequent increases in ecosystem respiration.

The effect of disturbance is poorly characterised in current land surface and global climate models [Running, 2008], it is therefore important to better understand how parameters and carbon pools might change following disturbance. DALEC2 and many other ecosystem models assume that respiration rates are proportional to carbon pool size. It has been suggested that although this assumption works well in equilibrium conditions it may not allow such models to predict ecosystem carbon dynamics following disturbance [Schimel and Weintraub, 2003]. The data assimilation techniques in this paper present a way for these simple models to cope with step changes in ecosystem behaviour, by allowing parameters and carbon pools to be updated following disturbance events.

5   Conclusion

In this work we have presented novel methods for understanding ecosystem responses to disturbance by using data assimilation. Assimilating all available data streams after an event of disturbance with a prior model prediction allows us to assess changes to model parameter and state variables due to this disturbance. We have also created modified observation operators to allow for the assimilation of daytime and nighttime NEE observations with a daily time-step model. This negates the need for model modification.

We find no significant change in net ecosystem carbon uptake after a thinning event in 2014 where approximately 46% of trees were removed from the studied area. This was also found to be true when a similar event occurred in 2007 [Wilkinson et al., 2015]. From our optimised model we find that reduced ecosystem respiration is the main reason for this unchanged net ecosystem carbon uptake. So that even for a demonstrated decrease in GPP following thinning, there is no significant change in NEE. We believe this reduction in ecosystem respiration is due to reduced input of autotrophic substrate following thinning, meaning both autotrophic and heterotrophic respiration are reduced. These results support work suggesting that GPP is the dominant driver for ecosystem respiration [Bhupinderpal et al., 2003, Heinemeyer et al., 2012, Högberg and Read, 2006, Janssens et al., 2001, Moore et al., 2013]. This has implications on future predictions of land surface carbon uptake and whether forests will continue to sequester atmospheric CO_2 at similar rates, or if they will be limited by increased GPP leading to increased respiration.

References

S. Bhupinderpal, A. Nordgren, M. Ottosson Löfvenius, M. N. Högberg, P. E. Mellander, and P. Högberg. Tree root and soil heterotrophic respiration as revealed by girdling of boreal scots pine forest: extending observations beyond the first year. *Plant, Cell & Environment*, 26(8):1287–1296, 2003. ISSN 1365-3040. doi: 10.1046/j.1365-3040.2003.01053.x. URL `http://dx.doi.org/10.1046/j.1365-3040.2003.01053.x`.

A. A. Bloom and M. Williams. Constraining ecosystem carbon dynamics in a data-limited world: integrating ecological "common sense" in a modeldata fusion framework. *Biogeosciences*, 12(5):1299–1315, 2015. ISSN 1726-4189. doi: 10.5194/bg-12-1299-2015. URL `http://www.biogeosciences.net/12/1299/2015/`.

N. J. Bréda. Ground-based measurements of leaf area index: a review of methods, instruments and current controversies. *Journal of experimental botany*, 54(392):2403–2417, 2003.

P. Ciais, C. Sabine, G. Bala, L. Bopp, V. Brovkin, J. Canadell, A. Chhabra, R. DeFries, J. Galloway, M. Heimann, et al. Carbon and other biogeochemical cycles. In *Climate change 2013: the physical science basis. Contribution of Working Group I to the Fifth Assessment Report of the Intergovernmental Panel on Climate Change*, pages 465–570. Cambridge University Press, 2014.

F. Dahdouh-Guebas and N. Koedam. Empirical estimate of the reliability of the use of the point-centred quarter method (pcqm): Solutions to ambiguous field situations and description of the pcqm+ protocol. *Forest Ecology and management*, 228(1):1–18, 2006.

F. A. Dijkstra and W. Cheng. Interactions between soil and tree roots accelerate long-term soil carbon decomposition. *Ecology Letters*, 10(11):1046–1053, 2007. ISSN 1461-0248. doi: 10.1111/j.1461-0248.2007.01095.x. URL `http://dx.doi.org/10.1111/j.1461-0248.2007.01095.x`.

S. Dore, M. Montes-Helu, S. C. Hart, B. A. Hungate, G. W. Koch, J. B. Moon, A. J. Finkral, and T. E. Kolb. Recovery of ponderosa pine ecosystem carbon and water fluxes from thinning and stand-replacing fire. *Global change biology*, 18(10):3171–3185, 2012.

K. S. Fassnacht, S. T. Gower, J. M. Norman, and R. E. McMurtric. A comparison of optical and direct methods for estimating foliage surface area index in forests. *Agricultural and Forest Meteorology*, 71(1):183–207, 1994.

A. Fox, M. Williams, A. D. Richardson, D. Cameron, J. H. Gove, T. Quaife, D. Ricciuto, M. Reichstein, E. Tomelleri, C. M. Trudinger, et al. The reflex project: comparing different algorithms and implementations for the inversion of a terrestrial ecosystem model against eddy covariance data. *Agricultural and Forest Meteorology*, 149(10):1597–1615, 2009.

J. Heath, E. Ayres, M. Possell, R. D. Bardgett, H. I. Black, H. Grant, P. Ineson, and G. Kerstiens. Rising atmospheric co2 reduces sequestration of root-derived soil carbon. *Science*, 309(5741): 1711–1713, 2005.

A. Heinemeyer, M. Wilkinson, R. Vargas, J.-A. Subke, E. Casella, J. I. Morison, and P. Ineson. Exploring the "overflow tap" theory: linking forest soil co2 fluxes and individual mycorrhizosphere components to photosynthesis. *Biogeosciences*, 9(1):79–95, 2012.

A. Hernesmaa, K. Bjrklf, O. Kiikkil, H. Fritze, K. Haahtela, and M. Romantschuk. Structure and function of microbial communities in the rhizosphere of scots pine after tree-felling. *Soil Biology and Biochemistry*, 37(4):777 – 785, 2005. ISSN 0038-0717. doi: http://dx.doi.org/10.1016/j.soilbio.2004.10.010. URL `http://www.sciencedirect.com/science/article/pii/S0038071704003918`.

T. Hilker, M. A. Wulder, N. C. Coops, J. Linke, G. McDermid, J. G. Masek, F. Gao, and J. C. White. A new data fusion model for high spatial-and temporal-resolution mapping of forest disturbance based on landsat and modis. *Remote Sensing of Environment*, 113(8):1613–1627, 2009.

P. Högberg and D. J. Read. Towards a more plant physiological perspective on soil ecology. *Trends in Ecology & Evolution*, 21(10):548–554, 2006.

P. Högberg, A. Nordgren, N. Buchmann, A. F. Taylor, A. Ekblad, M. N. Högberg, G. Nyberg, M. Ottosson-Löfvenius, and D. J. Read. Large-scale forest girdling shows that current photosynthesis drives soil respiration. *Nature*, 411(6839):789–792, 2001.

I. A. Janssens, H. Lankreijer, G. Matteucci, A. S. Kowalski, N. Buchmann, D. Epron, K. Pilegaard, W. Kutsch, B. Longdoz, T. Grnwald, L. Montagnani, S. Dore, C. Rebmann, E. J. Moors, A. Grelle, . Rannik, K. Morgenstern, S. Oltchev, R. Clement, J. Gumundsson, S. Minerbi, P. Berbigier, A. Ibrom, J. Moncrieff, M. Aubinet, C. Bernhofer, N. O. Jensen, T. Vesala, A. Granier, E. D. Schulze, A. Lindroth, A. J. Dolman, P. G. Jarvis, R. Ceulemans, and R. Valentini. Productivity overshadows temperature in determining soil and ecosystem respiration across european forests. *Global Change Biology*, 7(3):269–278, 2001. ISSN 1365-2486. doi: 10.1046/j.1365-2486.2001.00412.x. URL `http://dx.doi.org/10.1046/j.1365-2486.2001.00412.x`.

I. Jonckheere, S. Fleck, K. Nackaerts, B. Muys, P. Coppin, M. Weiss, and F. Baret. Review of methods for in situ leaf area index determination Part I. Theories, sensors and hemispherical

photography. *Agricultural and Forest Meteorology*, 121(1-2):19–35, 2004. ISSN 01681923. doi: 10.1016/j.agrformet.2003.08.027.

E. Kantzas, S. Quegan, and M. Lomas. Improving the representation of fire disturbance in dynamic vegetation models by assimilating satellite data: a case study over the arctic. *Geoscientific Model Development*, 8(8):2597–2609, 2015.

G. Kerr and J. Haufe. Thinning practice: A silvicultural guide. *Forestry Commission*, page 54, 2011.

J. Kimmins. Some statistical aspects of sampling throughfall precipitation in nutrient cycling studies in british columbian coastal forests. *Ecology*, pages 1008–1019, 1973.

W. A. Kurz, C. Dymond, G. Stinson, G. Rampley, E. Neilson, A. Carroll, T. Ebata, and L. Safranyik. Mountain pine beetle and forest carbon feedback to climate change. *Nature*, 452(7190):987–990, 2008.

A. S. Lawless. Variational data assimilation for very large environmental problems. In M. J. P. Cullen, M. A. Freitag, S. Kindermann, and R. Scheichl, editors, *Large scale Inverse Problems: Computational Methods and Applications in the Earth Sciences, Radon series on Computational and Applied Mathematics*, pages 55–90. De Gruyter, 2013.

S. Liu, B. Bond-Lamberty, J. A. Hicke, R. Vargas, S. Zhao, J. Chen, S. L. Edburg, Y. Hu, J. Liu, A. D. McGuire, J. Xiao, R. Keane, W. Yuan, J. Tang, Y. Luo, C. Potter, and J. Oeding. Simulating the impacts of disturbances on forest carbon cycling in north america: Processes, data, models, and challenges. *Journal of Geophysical Research: Biogeosciences*, 116(G4):n/a–n/a, 2011. ISSN 2156-2202. doi: 10.1029/2010JG001585. URL http://dx.doi.org/10.1029/2010JG001585. G00K08.

H. McKay, J. Hudson, and R. Hudson. Woodfuel resource in britain. *Forestry Commission Report*, 2003.

D. J. P. Moore, N. A. Trahan, P. Wilkes, T. Quaife, B. B. Stephens, K. Elder, A. R. Desai, J. Negron, and R. K. Monson. Persistent reduced ecosystem respiration after insect disturbance in high elevation forests. *Ecology Letters*, 16(6):731–737, 2013. ISSN 1461-0248. doi: 10.1111/ele.12097. URL http://dx.doi.org/10.1111/ele.12097.

V. Moreaux, É. Lamaud, A. Bosc, J.-M. Bonnefond, B. E. Medlyn, and D. Loustau. Paired comparison of water, energy and carbon exchanges over two young maritime pine stands (pinus pinaster ait.): effects of thinning and weeding in the early stage of tree growth. *Tree physiology*, page tpr048, 2011.

S. Niu, Y. Luo, M. C. Dietze, T. F. Keenan, Z. Shi, J. Li, and F. S. C. Iii. The role of data assimilation in predictive ecology. *Ecosphere*, 5(5):art65, 2014. ISSN 2150-8925. doi: 10.1890/ES13-00273.1. URL http://www.esajournals.org/doi/abs/10.1890/ES13-00273.1.

D. Papale, M. Reichstein, M. Aubinet, E. Canfora, C. Bernhofer, W. Kutsch, B. Longdoz, S. Rambal, R. Valentini, T. Vesala, et al. Towards a standardized processing of net ecosystem exchange measured with eddy covariance technique: algorithms and uncertainty estimation. *Biogeosciences*, 3(4):571–583, 2006.

A. Pierret, J.-L. Maeght, C. Clment, J.-P. Montoroi, C. Hartmann, and S. Gonkhamdee. Understanding deep roots and their functions in ecosystems: an advocacy for more unconventional research. *Annals of Botany*, 118(4):621–635, 2016. doi: 10.1093/aob/mcw130.

E. M. Pinnington, E. Casella, S. L. Dance, A. S. Lawless, J. I. Morison, N. K. Nichols, M. Wilkinson, and T. L. Quaife. Investigating the role of prior and observation error correlations in improving a model forecast of forest carbon balance using four-dimensional variational data assimilation. *Agricultural and Forest Meteorology*, 228229:299 – 314, 2016. ISSN 0168-1923. doi: http://dx.doi.org/10.1016/j.agrformet.2016.07.006.

T. Quaife, P. Lewis, M. De Kauwe, M. Williams, B. E. Law, M. Disney, and P. Bowyer. Assimilating canopy reflectance data into an ecosystem model with an Ensemble Kalman Filter. *Remote Sensing of Environment*, 112(4):1347–1364, 2008. ISSN 00344257. doi: 10.1016/j.rse.2007.05.020.

M. Raupach, P. Rayner, D. Barrett, R. DeFries, M. Heimann, D. Ojima, S. Quegan, and C. Schmullius. Model–data synthesis in terrestrial carbon observation: methods, data requirements and data uncertainty specifications. *Global Change Biology*, 11(3):378–397, 2005.

P. M. Rich, J. Wood, D. Vieglais, K. Burek, and N. Webb. Hemiview user manual, version 2.1. *Delta-T Devices Ltd., Cambridge, UK*, 79, 1999.

A. D. Richardson, M. D. Mahecha, E. Falge, J. Kattge, A. M. Moffat, D. Papale, M. Reichstein, V. J. Stauch, B. H. Braswell, G. Churkina, B. Kruijt, and D. Y. Hollinger. Statistical properties of random {CO2} flux measurement uncertainty inferred from model residuals. *Agricultural and Forest Meteorology*, 148(1):38 – 50, 2008. ISSN 0168-1923. doi: http://dx.doi.org/10.1016/j.agrformet.2007.09.001.

A. D. Richardson, M. Williams, D. Y. Hollinger, D. J. Moore, D. B. Dail, E. A. Davidson, N. A. Scott, R. S. Evans, H. Hughes, J. T. Lee, et al. Estimating parameters of a forest ecosystem c model with measurements of stocks and fluxes as joint constraints. *Oecologia*, 164(1):25–40, 2010.

S. W. Running. Ecosystem disturbance, carbon, and climate. *Science*, 321(5889):652–653, 2008.

J. P. Schimel and M. N. Weintraub. The implications of exoenzyme activity on microbial carbon and nitrogen limitation in soil: a theoretical model. *Soil Biology and Biochemistry*, 35(4):549–563, 2003.

R. Seidl, P. M. Fernandes, T. F. Fonseca, F. Gillet, A. M. Jönsson, K. Merganičová, S. Netherer, A. Arpaci, J.-D. Bontemps, H. Bugmann, et al. Modelling natural disturbances in forest ecosystems: a review. *Ecological Modelling*, 222(4):903–924, 2011.

J. Talbot, S. Allison, and K. Treseder. Decomposers in disguise: mycorrhizal fungi as regulators of soil c dynamics in ecosystems under global change. *Functional ecology*, 22(6):955–963, 2008.

P. Thornton, B. Law, H. L. Gholz, K. L. Clark, E. Falge, D. Ellsworth, A. Goldstein, R. Monson, D. Hollinger, M. Falk, et al. Modeling and measuring the effects of disturbance history and climate on carbon and water budgets in evergreen needleleaf forests. *Agricultural and forest meteorology*, 113(1):185–222, 2002.

Y. Tremolet. Accounting for an imperfect model in 4D-Var. *Quarterly Journal of the Royal Meteorological Society*, 132(621):2483–2504, 2006. ISSN 00359009. doi: 10.1256/qj.05.224. URL http://doi.wiley.com/10.1256/qj.05.224.

T. Vesala, T. Suni, Ü. Rannik, P. Keronen, T. Markkanen, S. Sevanto, T. Grönholm, S. Smolander, M. Kulmala, H. Ilvesniemi, et al. Effect of thinning on surface fluxes in a boreal forest. *Global Biogeochemical Cycles*, 19(2), 2005.

M. Wilkinson, E. Eaton, M. Broadmeadow, and J. Morison. Inter-annual variation of carbon uptake by a plantation oak woodland in south-eastern england. *Biogeosciences*, 9(12):5373–5389, 2012.

M. Wilkinson, P. Crow, E. Eaton, and J. Morison. Effects of management thinning on co_2 exchange by a plantation oak woodland in south-eastern england. *Biogeosciences Discussions*, 12(19), 2015.

M. Williams, E. B. Rastetter, D. N. Fernandes, M. L. Goulden, G. R. Shaver, and L. C. Johnson. Predicting gross primary productivity in terrestrial ecosystems. *Ecological Applications*, 7(3): 882–894, 1997.

M. Williams, P. A. Schwarz, B. E. Law, J. Irvine, and M. R. Kurpius. An improved analysis of forest carbon dynamics using data assimilation. *Global Change Biology*, 11(1):89–105, 2005.

J. Zobitz, A. Desai, D. Moore, and M. Chadwick. A primer for data assimilation with ecological models using markov chain monte carlo (mcmc). *Oecologia*, 167(3):599–611, 2011.

J. M. Zobitz, D. J. P. Moore, T. Quaife, B. H. Braswell, A. Bergeson, J. a. Anthony, and R. K. Monson. Joint data assimilation of satellite reflectance and net ecosystem exchange data constrains ecosystem carbon fluxes at a high-elevation subalpine forest. *Agricultural and Forest Meteorology*, 195-196:73–88, 2014. ISSN 01681923. doi: 10.1016/j.agrformet.2014.04.011. URL `http://dx.doi.org/10.1016/j.agrformet.2014.04.011`.

Appendix

6 DALEC2 equations

The model equations for the carbon pools at day i are as follows:

$$GPP^i = ACM(C_{fol}^{i-1}, c_{lma}, c_{eff}, \Psi) \tag{5}$$

$$C_{lab}^i = C_{lab}^{i-1} + (1 - f_{auto})(1 - f_{fol})f_{lab}GPP^i - \Phi_{on}C_{lab}^{i-1}, \tag{6}$$

$$C_{fol}^i = C_{fol}^{i-1} + \Phi_{on}C_{lab}^{i-1} + (1 - f_{auto})f_{fol}GPP^i - \Phi_{off}C_{fol}^{i-1}, \tag{7}$$

$$C_{roo}^i = C_{roo}^{i-1} + (1 - f_{auto})(1 - f_{fol})(1 - f_{lab})f_{roo}GPP^i - \theta_{roo}C_{roo}^{i-1}, \tag{8}$$

$$C_{woo}^i = C_{woo}^{i-1} + (1 - f_{auto})(1 - f_{fol})(1 - f_{lab})(1 - f_{roo})GPP^i - \theta_{woo}C_{woo}^{i-1}, \tag{9}$$

$$C_{lit}^i = C_{lit}^{i-1} + \theta_{roo}C_{roo}^{i-1} + \Phi_{off}C_{fol}^{i-1} - (\theta_{lit} + \theta_{min})e^{\Theta T^{i-1}}C_{lit}^{i-1}, \tag{10}$$

$$C_{som}^i = C_{som}^{i-1} + \theta_{woo}C_{woo}^{i-1} + \theta_{min}e^{\Theta T^{i-1}}C_{lit}^{i-1} - \theta_{som}e^{\Theta T^{i-1}}C_{som}^{i-1}, \tag{11}$$

where T^{i-1} is the daily mean temperature, Ψ represents the meteorological driving data used in the GPP function and Φ_{on}/Φ_{off} are functions controlling leaf-on and leaf-off. Descriptions for each model parameter used in equations (5) to (11) are included in table 3. DALEC2 can be parameterised for both deciduous and evergreen sites with Φ_{on} and Φ_{off} being able to reproduce the phenology of either type of site. The full details of this version of DALEC can be found in Bloom and Williams [2015].

7 Observation error covariance matrices
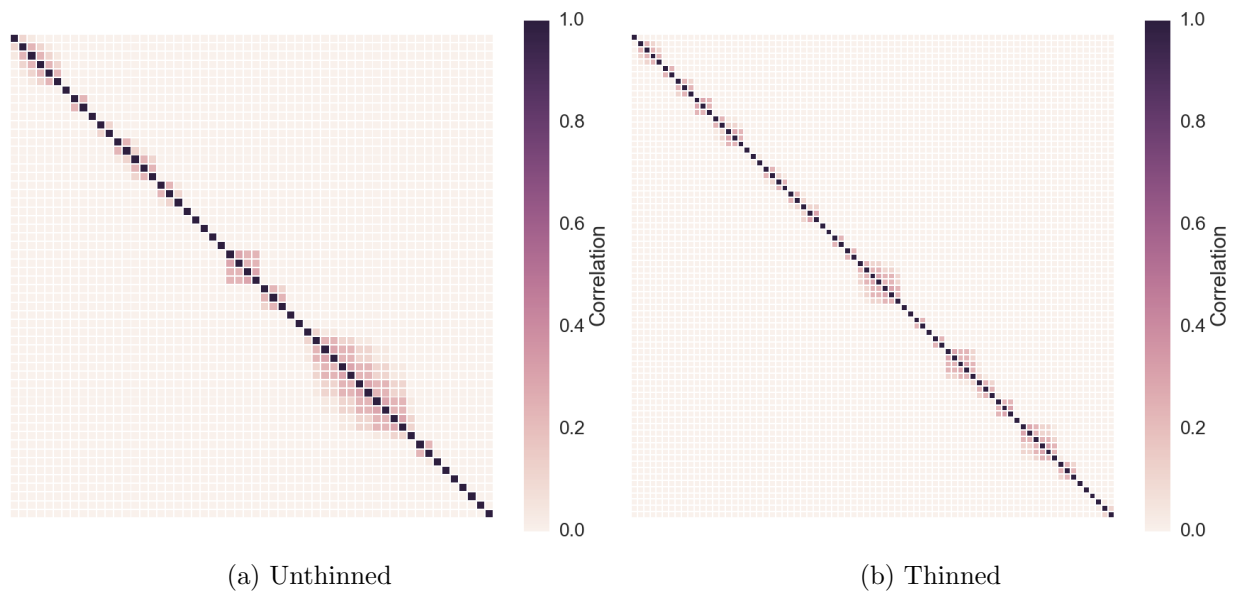

(a) Unthinned

(b) Thinned

Figure 6: Observation error correlation matrices for thinned and unthinned data assimilation experiments. For more details see Pinnington et al. [2016]

Parameter	Description	Background vector ($\mathbf{x}^b$)	Standard deviation	Range
θ_{min}	Litter mineralisation rate (day^{-1})	9.810×10^{-4}	2.030×10^{-3}	$10^{-5} - 10^{-2}$
f_{auto}	Autotrophic respiration fraction	5.190×10^{-1}	1.168×10^{-1}	$0.3 - 0.7$
f_{fol}	Fraction of GPP allocated to foliage	1.086×10^{-1}	1.116×10^{-1}	$0.01 - 0.5$
f_{roo}	Fraction of GPP allocated to fine roots	4.844×10^{-1}	2.989×10^{-1}	$0.01 - 0.5$
c_{lspan}	Determines annual leaf loss fraction	1.200×10^{0}	1.161×10^{-1}	$1.0001 - 10$
θ_{woo}	Woody carbon turnover rate (day^{-1})	1.013×10^{-4}	1.365×10^{-4}	$2.5 \times 10^{-5} - 10^{-3}$
θ_{roo}	Fine root carbon turnover rate (day^{-1})	3.225×10^{-3}	2.930×10^{-3}	$10^{-4} - 10^{-2}$
θ_{lit}	Litter carbon turnover rate (day^{-1})	3.442×10^{-3}	3.117×10^{-3}	$10^{-4} - 10^{-2}$
θ_{som}	Soil and organic carbon turnover rate (day^{-1})	1.113×10^{-4}	1.181×10^{-4}	$10^{-7} - 10^{-3}$
Θ	Temperature dependance exponent factor	4.147×10^{-2}	1.623×10^{-2}	$0.018 - 0.08$
c_{eff}	Canopy efficiency parameter	7.144×10^{1}	2.042×10^{1}	$10 - 100$
d_{onset}	Leaf onset day (day)	1.158×10^{2}	6.257×10^{0}	$1 - 365$
f_{lab}	Fraction of GPP allocated to labile carbon pool	3.204×10^{-1}	1.145×10^{-1}	$0.01 - 0.5$
c_{ronset}	Labile carbon release period (days)	4.134×10^{1}	1.405×10^{1}	$10 - 100$
d_{fall}	Leaf fall day (day)	2.205×10^{2}	3.724×10^{1}	$1 - 365$
c_{rfall}	Leaf-fall period (days)	1.168×10^{2}	2.259×10^{1}	$10 - 100$
c_{lma}	Leaf mass per area (g C m^{-2})	1.285×10^{2}	6.410×10^{1}	$10 - 400$
C_{lab}	Labile carbon pool (g C m^{-2})	1.365×10^{2}	6.626×10^{1}	$10 - 1000$
C_{fol}	Foliar carbon pool (g C m^{-2})	6.864×10^{1}	3.590×10^{1}	$10 - 1000$
C_{roo}	Fine root carbon pool (g C m^{-2})	2.838×10^{2}	2.193×10^{2}	$10 - 1000$
C_{woo}	Above and below ground woody carbon pool (gCm^{-2})	6.506×10^{3}	7.143×10^{3}	$100 - 10^{5}$
C_{lit}	Litter carbon pool (g C m^{-2})	5.988×10^{2}	5.450×10^{2}	$10 - 1000$
C_{som}	Soil and organic carbon pool (g C m^{-2})	1.936×10^{3}	1.276×10^{3}	$100 - 2 \times 10^{5}$

Table 3: Parameter values and standard deviations for background vector used in experiments.